2D numerical study of circular synthetic jets in quiescent flows

H. Tang and S. Zhong
School of Mechanical, Aerospace and Civil Engineering,
The University of Manchester, UK

ABSTRACT

2D numerical simulations of flows generated by a synthetic jet actuator with a circular orifice were conducted at two different diaphragm displacement settings, one representing a typical laminar case and the other a fully turbulent case. The flow in the cavity was included in the computation in order to provide more accurate predictions. A velocity boundary condition was applied at the neutral position of the diaphragm to account for its temporal deformation. Comparisons were made between the computational results and existing PIV and hot-wire data in terms of the time sequence of the velocity vector field, velocity variations in space and with time. It is found that computational results for the laminar case agree well with the experimental data. Four turbulent models were tested for the fully turbulent case. It was found that the predictions using the RNG κ-ε and Standard κ-ε models were reasonably close to the experimental data. This initial study has produced some encouraging evidence for the capacity of FLUENT in simulating the key features of synthetic jets.

NOMENCLATURE

D_c	diaphragm/cavity diameter, mm
D_o	orifice diameter, mm
f	diaphragm oscillation frequency, Hz
h	orifice depth, mm
H	cavity height, mm
r	radical distance from the centre of diaphragm, mm
t	time, sec
T	period of a diaphragm oscillation cycle, sec
u	velocity of diaphragm movement, mm/sec
U_{peak}	peak velocity at orifice exit, m/sec
x	axial distance from orifice exit, mm
δ	deformation of diaphragm, mm
Δ	peak-to-peak displacement at the centre of diaphragm, mm
Δt	time step used in the simulation, sec

1.0 INTRODUCTION

Synthetic jets have been a hot research topic since mid 1990s due to a renewed interest in flow control and their potential use in aircraft applications, such as separation delay[1-3]. The primary advantage is that they are massless jets hence unlike steady or pulsed jets they do not require a compressed air supply and its auxiliary equipment which would carry a weight penalty.

A typical synthetic jet actuator, as shown in Fig. 1, consists of a small cavity with a vibrating diaphragm at its bottom side and an orifice plate at the opposite side. During a downward motion of the diaphragm the surrounding air is drawn into the cavity. When the diaphragm is moving upward, the fluid in the cavity is expelled through the orifice producing a vortex ring at the exit of the orifice. Repeating this process at a certain frequency produces a succession of vortices which propagate away from the orifice. The characteristics and interaction of the train of vortices can be varied by changing the amplitude, frequency of the diaphragm motion and orifice geometry[4]. It is believed that interaction of these vortices with the local boundary layer produces streamwise vortcial structures which are capable of delaying flow separation by entraining high speed fluids from the freestream to the near wall region[5].

In order to assist the design of synthetic jet actuators for flow control purposes, computational capability of accurately predicting the characteristics of synthetic jets is sought. Validation of computa-

Paper No. 2938. Manuscript received 14 October 2004 accepted 30 November 2004.

https://doi.org/10.1017/S0001924000000592 Published online by Cambridge University Press

tional models against existing experimental data hence becomes an integrated part of this development. This would add confidence in the use of the computational models in cases where experimental data are not available.

In recent years, synthetic jets produced through high aspect ratio rectangular orifices in quiescent and cross flows have been studied intensively due to their predominant two-dimensional nature in the near field. The experimental results obtained by Smith and Glezer[1] became the database for the validation of many numerical investigations[6-8]. However to date the computational modelling of circular synthetic jets is still scarce. Compared with rectangular jets, circular jets are more attractive in flow control applications on aircraft, especially in microelectronic mechanical systems (MEMS) based devices, because they are space saving and easily arrayed.

To the best knowledge of the authors, the most comprehensive validation of circular synthetic jets reported so far was undertaken by Mallinson *et al*[9]. The simulation was performed using CFX for turbulent synthetic jets in quiescent conditions and the results were validated using their own hot wire data. To simplify the computation, the cavity was omitted and only a velocity boundary condition was applied at the orifice exit plane. The velocity boundary condition was adjusted until the time-averaged velocity at the jet centreline has the closest possible match to the experimental results in the far field. According to Rizzetta *et al*[7], however, significant differences in velocity time history at the centreline could occur when the cavity flow was neglected.

Although the cavity was included and a moving boundary condition was applied at the neutral position of the diaphragm in Mallinson's recent work[10], the validation was carried out mainly along the centreline of the jet using time averaged data. Due to the oscillation of the diaphragm, the flowfield is unsteady as the result of periodic formation and advection of vortex rings from the orifice exit. Accurate reproduction of the key features of the unsteady flow associated with the vortex rings using computational models is hence essential. Validation of the simulation results requires the availability of full field experimental data obtained at different phases of the diaphragm oscillation cycle. To this end time-averaged data acquired at discrete points appear to be insufficient to serve this purpose.

Research work on synthetic jets has been undertaken at the Goldstein Aeronautical Laboratory at the University of Manchester for many years. Following an initial success in demonstrating the ability of synthetic jets in delaying flow separation on a circular cylinder model at a Reynolds number of 5×10^6, experiments have been carried out to understand the fundamental fluid mechanics of synthetic jets under different actuator geometry and operating conditions at quiescent conditions[4]. Sets of PIV data of circular synthetic jets at different phases of diaphragm oscillation cycle have been acquired which provide a unique database for validating CFD simulation results. In this paper, an initial effort of making use of this database to validate the results from a commercial software FLUENT is reported. In order to ensure the accuracy of the numerical results, the cavity was included in the simulation and a velocity boundary condition is applied at the neutral position of the diaphragm using the membrane theory.

2.0 EXPERIMENTAL METHOD

The synthetic jet actuator used in this study consists of a cylindrical cavity, a diaphragm made of a thin steel shim and a cap with an orifice opening (see Fig. 1). The orifice has a diameter D_o of 5mm and a height h of 5mm. The cavity inner diameter D_c is 45mm, and its height H is 10mm. The diaphragm is attached via a steel rod to a permanent magnetic shaker which is driven by a sine wave from a signal generator unit.

The PIV measurements were conducted using a frequency doubled Q-switched Nd:Yag laser and a CCD camera operated at 10

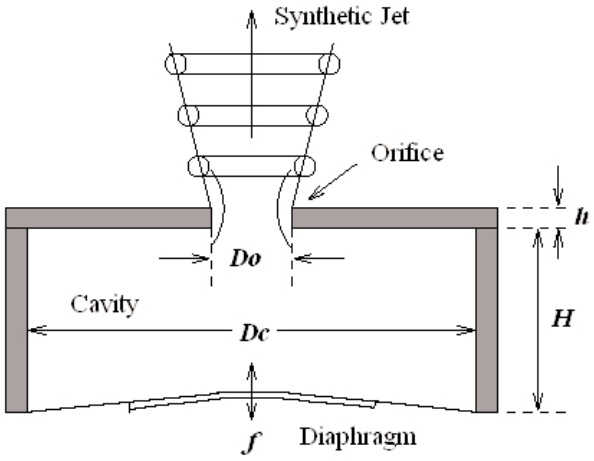


Figure 1. Schematic diagram of a synthetic jet actuator.

Hz with a resolution of 1000 × 1016 pixels. The seeding was produced by suspending a heated wire inside the cavity and dripping Shell Ondena oil down it. The laser sheet was perpendicular to the orifice plate through the central plane of the orifice. With this setup a three-dimensional vortex ring would appear as a two-dimensional vortex 'pair' in the recorded images. A two-frame cross-correlation algorithm was used to deduce the velocity vectors from PIV images.

In order to carry out the measurement at given phases of the diaphragm oscillation cycle, the image recording system was synchronised with the motion of the diaphragm. In the present experiment, the system was set up such that images were taken at 16 equally spaced phases during the diaphragm oscillation cycle.

To ensure adequate spatial resolution of the flow structures, the PIV measurements were made within a region of 25mm by 25mm. Due to scattering of laser light from the orifice plate, there is no PIV data within a distance of about 2mm from the orifice exit plane. Hence a hot wire of 1mm in length was used to provide supplementary data at the centre of the exit plane.

During the experiment, the diaphragm oscillating frequency f was fixed at 50Hz and the diaphragm peak-to-peak displacement Δ was varied between 0·3mm and 1·1mm. The diaphragm displacement was measured with an eddy-current displacement sensor. Increasing the diaphragm displacement will yield a higher jet velocity. As shown in the smoke visualisation pictures (Fig. 2), the synthetic jet appears to be laminar as it just emerges from the orifice. But as the displacement increases to 0·8mm, the jet becomes turbulent after about two orifice diameters from the exit.

3.0 COMPUTATIONAL METHOD

Figure 3 illustrates the computational geometry and mesh used in the present study. The mesh size and spacing are given in Table 1. Since the flow can be assumed to be axisymmetric, only the top half of the flow field is calculated. The slight non-axisymmetry showed in the smoke visualisation pictures (Fig. 2) was caused by the buoyancy effect experienced by the vapourised oil which was used to make the jet visible.

The boundary conditions are also indicated in Fig. 3. For simplification, a velocity-inlet boundary condition is applied at the neutral position of the diaphragm instead of a moving boundary condition. As the jet exit velocity strongly depends on the mass flux displaced by the diaphragm motion, the profile of diaphragm deformation affects the accuracy of the simulation. In the present experimental

https://doi.org/10.1017/S0001924000000592 Published online by Cambridge University Press

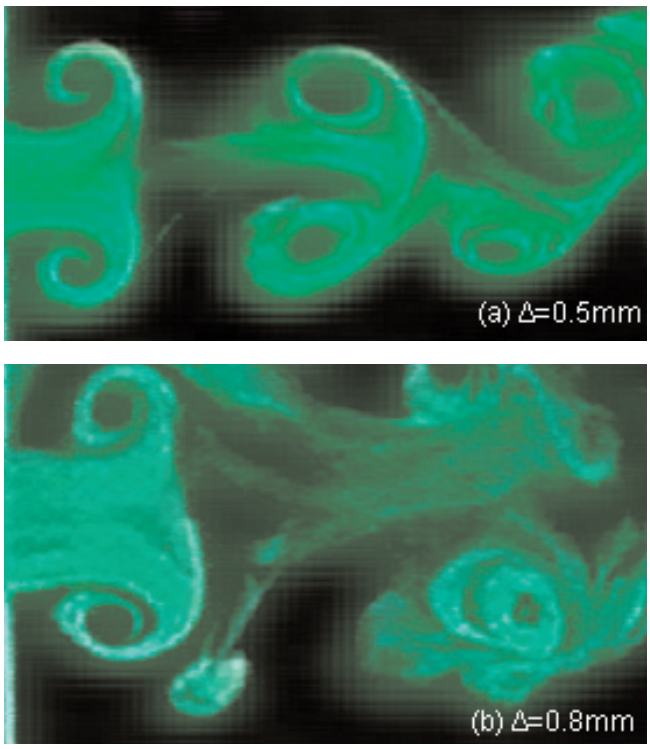


Figure 2. Smoke visualisation of synthetic jets produced with two different diaphragm displacements.

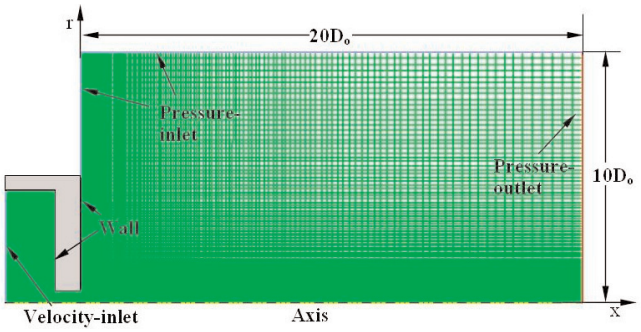


Figure 3. Computational geometry and mesh.

setup, the diaphragm is clamped around its circular edge and the displacement at the centre of the diaphragm is fixed at a known value. According to the theory of plates and shells[11], for such a case the instantaneous shape of the oscillating diaphragm is described as:

$$\delta(r,t)=\frac{\Delta}{2}\left[1-\frac{4r^2}{D_c^2}+\frac{8r^2}{D_c^2}\ln\left(\frac{2r}{D_c}\right)\right]\mathrm{Cos}(2\pi ft) \quad \ldots (1)$$

where δ is the diaphragm deformation relative to its neutral position, r is the distance from the centre of the diaphragm and Δ is the peak-to-peak displacement at the centre of the diaphragm. The derivative of Equation (1) with time gives the moving velocity of the diaphragm

Table 1
Computation mesh parameters

Mesh zone	Mesh size	Δx_{min}(mm)	Δy_{min}(mm)
Cavity	50 × 105	0·2	0·1
Orifice	50 × 25	0·1	0·1
Outer zone	143×120	0·125	0·1

Table 2
Mesh refinement cases

Mesh designation	Coarse	Medium	Fine
Cavity	25 × 52	50 × 105	100 × 210
Orifice	25 × 12	50 × 25	100 × 50
Outer zone	71 × 60	143 × 120	286 × 240

$$u(r,t)=\pi\Delta f\left[1-\frac{4r^2}{D_c^2}+\frac{8r^2}{D_c^2}\ln\left(\frac{2r}{D_c}\right)\right]\mathrm{Sin}(2\pi ft) \quad \ldots (2)$$

Unsteady 2D axisymmetric incompressible numerical simulations were performed using a commercial solver FLUENT 6.1, which is based on the finite-volume formulation. The second-order upwind scheme was selected in space discretisation and the first-order implicit scheme in time. The pressure correction was obtained using the pressure-implicit with splitting of operators (PISO) method, which moves the repeated calculations required by SIMPLE and SIMPLEC inside the solution stage of the pressure-correction equation and this method is more suitable for transient calculations.

4.0 CHOICES OF MESH SIZE AND TIME STEP

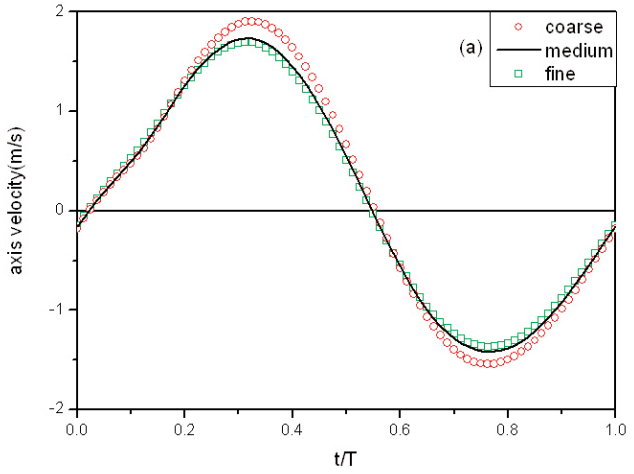
Before the final computational results were produced, the sensitivity of the results to the choices of mesh size and time step was investigated. The main purpose of this investigation is to determine the minimal number of mesh points and time steps necessary to obtain solutions of acceptable accuracy in the regions of interest. All these tests were carried out for the case of diaphragm peak-to-peak displacement Δ = 0·5mm. The effects of mesh size and time step were evaluated in terms of the variation of axial velocity at the orifice exit and vorticity distributions.

Three meshes as specified in Table 2, were used in the mesh refinement study. The axial velocity variations at the orifice exit using these three meshes are shown in Fig. 4(a). The mesh density appears to have a larger effect on the solution where the velocity magnitude is larger. The maximum velocity obtained from the medium mesh and the coarse mesh differs from that of the finest mesh by about 2% and 12% respectively. As a compromise between accuracy of results and computational time, the medium mesh was used to compute the final results.

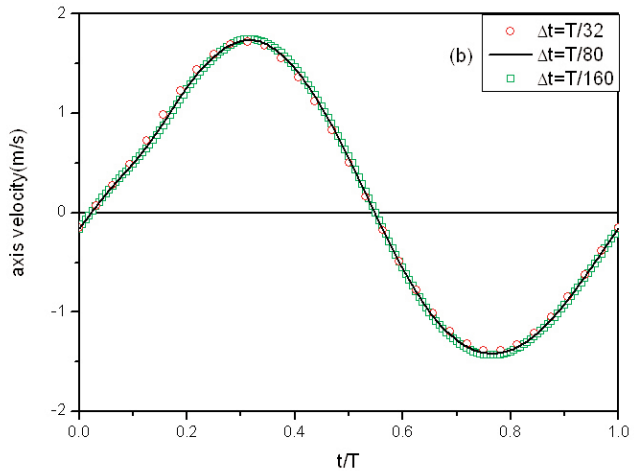
In the time-step refinement study the Δ = 0·5mm case with a medium mesh was solved using different time steps: $\Delta t = T/32$, $T/80$ and $T/160$. The axial velocity variations at the orifice exit obtained using these time steps are shown in Fig. 4(b). It appears that the velocity is not sensitive to the range of time-step magnitudes tested here. The velocity obtained for the medium time-step of $T/80$ deviates by less than 1% from that of the finest time-step of $T/160$, indicating that the choice of the medium time-step would be adequate.

Finally instantaneous vorticity contours produced using combinations of the fine time-step with the fine mesh and the medium time-step with the medium mesh respectively were compared (see Fig. 5).

https://doi.org/10.1017/S0001924000000592 Published online by Cambridge University Press



(a)



(b)

Figure 4. Comparison of axial velocity at the centre of orifice exit in a cycle produced (a) using different mesh densities; (b) using different time-steps.

Although there is a slight difference in vorticity values, the size and shape of the vortices inside and outside the cavity in both cases appear to be almost the same. Since the induced convective velocity of the vortices strongly depends on the solution, the fact that the vortices appear to have propagated almost the same distance over the same time period in both cases suggests that the accumulated discrepancy due to the choice of time step and mesh density is negligible. This evidence again indicates that the solution is adequate when the medium time-step and medium mesh are used. Hence medium time-step and medium mesh were employed in this study to produce the results presented here.

5.0 RESULTS AND DISCUSSION

Although PIV data are available for nine diaphragm peak-to-peak displacements from 0·3 to 1·1mm, only the detailed comparisons between experimental and simulation results for Δ = 0·5mm (Case 1) and Δ = 0·8mm (Case 2) are presented in this paper. According to the smoke visualisation experimental results (see Fig. 2), in Case 1 the flow is laminar, whereas in Case 2 the flow becomes turbulent after $x = 2D_o$. The choice of these two cases would allow the capability of FLUENT in simulating laminar and turbulent synthetic jets to be assessed. The comparison between the simulation and experimental data is confined to the near field of the synthetic jets ($x < 5D_o$) where PIV data are available. Nevertheless such a comparison is still meaningful since it is the near field behaviour of synthetic jets that is of particular interest for flow control of boundary layers.

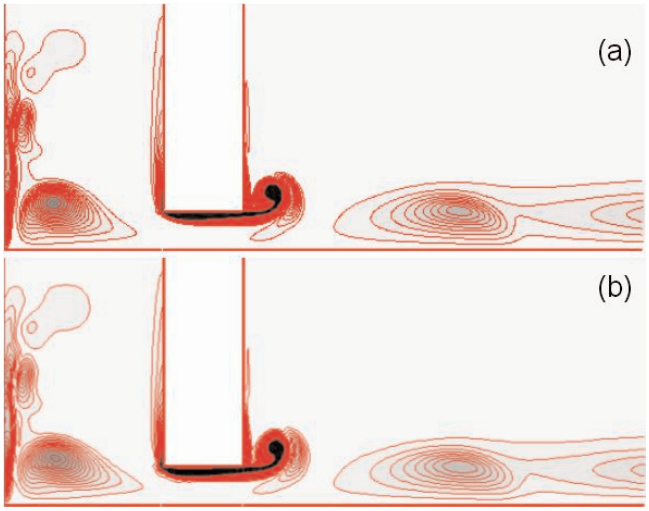


Figure 5. Instantaneous vorticity contours at t/T = 5/16. (a) Fine mesh, $\Delta t = T/160$; (b) Medium mesh, $\Delta t = T/80$. 25 contour levels are displayed between 0 and 2000s^{-1}.

5.1 Case 1: Synthetic jets produced with a diaphragm displacement of Δ = 0·5mm

This case was computed using the laminar model. Figure 6 shows the comparison of a time sequence of velocity vectors between the PIV data and the computational results. This time sequence shows the formation and evolution of vortex rings. Since in the PIV experiments the seeding particles were released from the cavity, the experimental data were confined to the region where seeding particles were present. The simulation appears to recreate the vortical structure similar to that revealed by PIV data especially near the exit of the orifice.

Figure 7 shows the comparison between the measured and predicted variations of velocity magnitudes at the centre of the orifice exit plane during a diaphragm vibration cycle. Here t/T = 0 corresponds to the instant when the blowing part of the cycle begins. During the diaphragm oscillation cycle there are two velocity peaks, the larger peak occurs during the blowing cycle and the smaller peak in the suction cycle. The absolute velocity associated with the second peak is supposed to be negative. Since the experimental data were obtained using a hot wire which is not able to differentiate if the flow is going into or coming out from the orifice, the velocity magnitude is presented here. Due to the existence of a cavity, these two peaks lag behind the peaks of diaphragm oscillating velocity (shown as the dashed line). The computational result shows the same trend as the hot wire data. The magnitude of the predicted maximum velocity in the blowing cycle is about 10% larger than the measurement, which is quite acceptable. However, there is a phase difference between the predicted and measured velocity. In the first half of the blowing cycle the predicted velocity lags behind the experimental data, whereas in the first half of the suction cycle the trend is reversed. The reason behind this deviation needs to be investigated.

https://doi.org/10.1017/S0001924000000592 Published online by Cambridge University Press

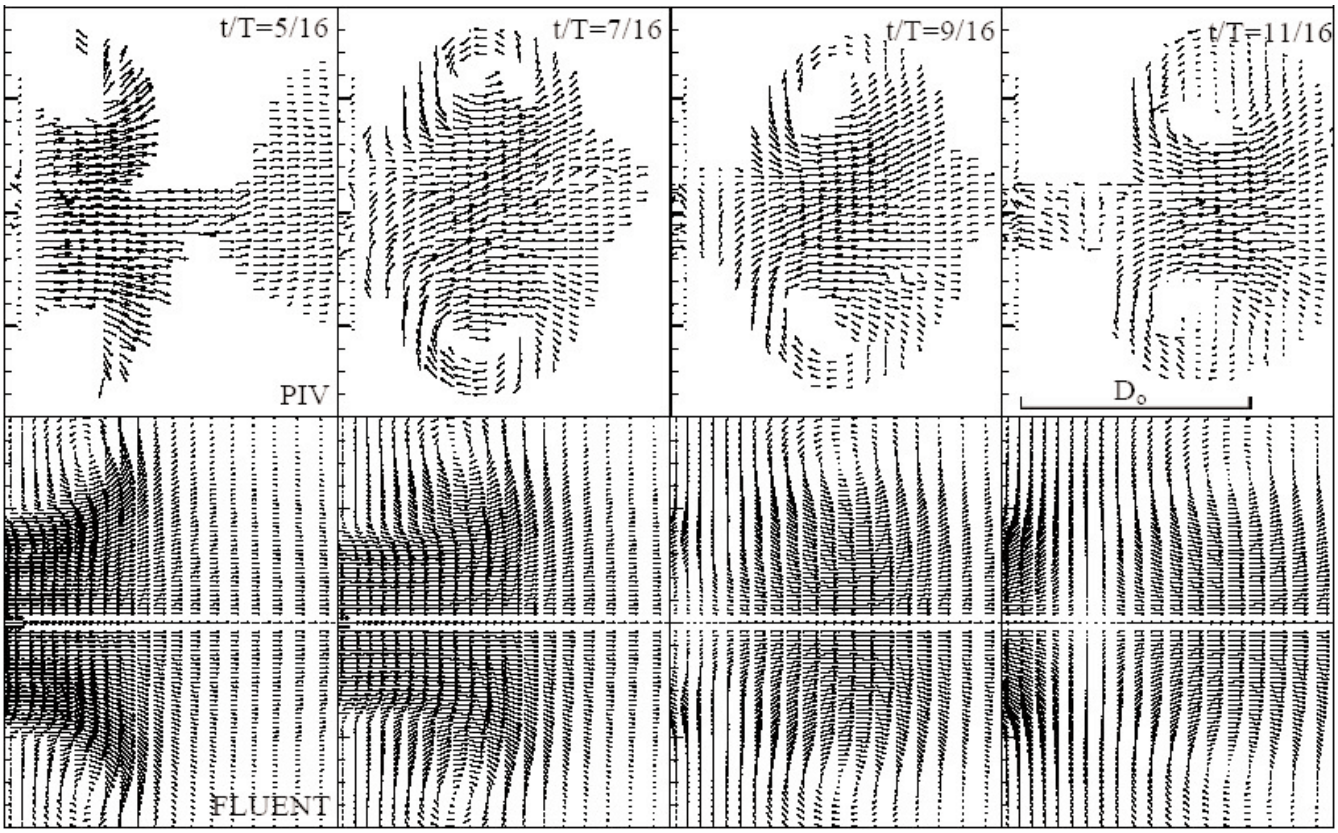


Figure 6. Time sequence of velocity vectors

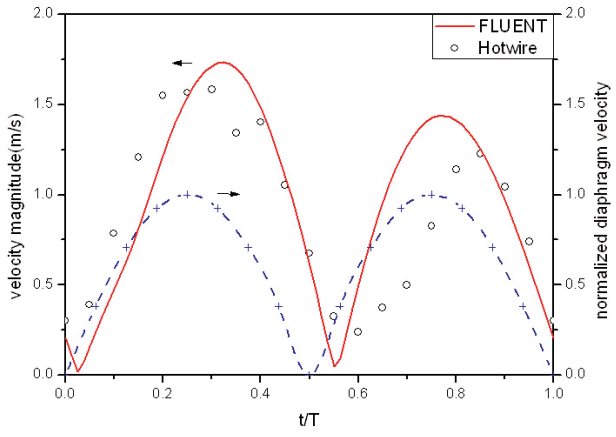


Figure 7. Variation of velocity magnitude at the centre of the orifice exit plane during a cycle (Case 1).

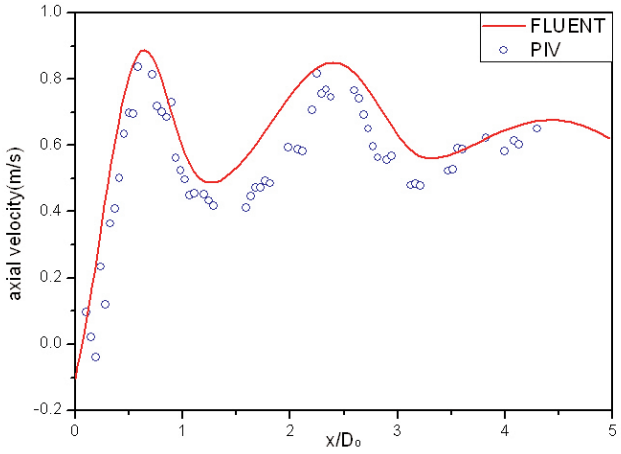


Figure 8. Instantaneous centreline velocity (Case 1: $t/T = 9/16$).

Instantaneous velocity distributions along the centreline and in the spanwise direction are also compared with the PIV data. Figure 8 shows the axial velocity along the centreline at $t/T = 9/16$. The x-coordinate corresponds to the axial distance away from the orifice exit, which ranged between 0 to $5D_o$. Although the velocity magnitudes are slightly larger, the computation results appear to follow the PIV data closely showing three distinct peaks which correspond to the locations of consecutive vortex rings. The instantaneous axial velocity profile at $t/T = 14/16$ across the span of the jet at $x = 1D_o$ is shown in Fig. 9. The time instant was chosen such that the vortex cores arrive at this streamwise location. Although the predicted velocity is slightly larger than the measured values, the agreement between the prediction and measurement is reasonable.

https://doi.org/10.1017/S0001924000000592 Published online by Cambridge University Press

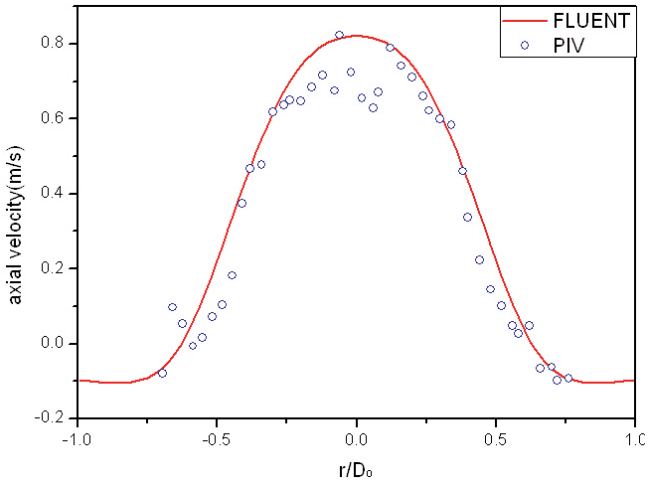


Figure 9. Velocity profile at $x = 1D_o$ (Case 1: $t/T = 14/16$).

5.2 Case 2: Synthetic jets produced with a diaphragm displacement of Δ = 0·8mm

It is seen that the synthetic jet produced with a peak-to-peak diaphragm oscillation displacement of 0·8mm becomes turbulent at a small distance from the orifice. It is a complex flow including both laminar and turbulent regions. However, since FLUENT does not include a transition model, it is not possible to compute laminar and turbulent flow in different regions simultaneously in FLUENT. In the present study, a turbulence model with low turbulent intensity has to be used to reproduce the key characteristics of the flow. Four turbulent models, i.e. Standard κ-ε, RNG κ-ε, Standard κ-ω and Reynolds stress (RSM) models were used with the solver in order to see which model gives the closest match to the experimental data. The first three models are all two-equation models, whereas the RSM model is a second-moment closure model.

Firstly, the instantaneous velocity distributions along the centreline of the jet are compared. Figure 10 shows instantaneous axial velocities along the centreline during the blowing part of the cycle at $t/T = 5/16$ and 7/16. Except for the Standard κ-ε model, the other three models show a similar trend as the PIV data. The velocity magnitudes are close to the PIV data at the two velocity peaks located around $x = 0{\cdot}5D_o$ and $5D_o$ at $t/T = 5/16$. However, the models over-predicted the axial velocity in the region between the two peaks.

Secondly, it is also found that except for the standard κ-ε model the other three models, especially the RNG κ-ε model and Standard κ-ω model, produce a close match to the experimental data in the region $x < 1D_o$. The velocity profiles across the jet at $x = 1D_o$ are plotted in Fig. 11. The results of the Standard κ-ε model appear to depart significantly from the experimental data near the centreline. A considerable difference between the prediction and PIV data at $t/T = 5/16$ also exists when the RSM model is used.

The reason that the Standard κ-ε model produces the least satisfactory results is because it does not model the subtle effects of streamline curvature on turbulence and hence it is less capable of dealing with flows with large, rapid changing strain rates. Overall it is concluded that the RNG κ-ε model and standard κ-ω model outperform other turbulent models. In this study, the RNG κ-ε model was chosen as the turbulent model for later analyses.

With the use of the RNG κ-ε turbulent model, a good agreement in velocity magnitudes between the computational and the hot-wire results at the centre of the orifice exit plane is also achieved except for a small phase difference which is similar to that observed in Case 1 (see Fig. 12).

The comparison of a time sequence of velocity vectors between the simulation, which is computed with the RNG κ-ε model, and the PIV data is shown in Fig. 13. Due to the larger oscillation amplitude of the diaphragm, the vortex ring appears to have a much bigger vortex core and to advect faster than the laminar vortex ring in Case 1. The simulation seems to have reproduced the flow structures observed in the experiment in terms of their shape and position. This indicates that the turbulent simulation is quite successful in the near field of the synthetic jets.

6.0 OTHER COMPARISONS

One of the key parameters that characterises the performance of a synthetic jet actuator is the peak velocity at the jet exit plane. The velocity can be used to calculate the Reynolds number that characterises the synthetic jet flow.

Nine cases, in which the diaphragm peak-to-peak displacement varied from 0·3mm to 1·1mm, were computed using the laminar model in order to obtain the predicted peak velocity at the centre of the orifice. The laminar model is acceptable for this purpose because based on experimental observations the flow appears to show laminar features near the orifice exit in all the cases. The predictions are compared with the PIV data in Fig. 14. The PIV data were obtained 2mm away from the orifice. It can be seen that except for two cases ($\Delta/D_o = 0{\cdot}12$ and 0·14), the computational results agree with the PIV data very well, indicating that the computational models are capable of accurately predicting the jet peak exit velocity.

The streamwise trajectories of vortex cores during an oscillation cycle for Case 1 and Case 2 are shown in Fig. 15. The experimental results show that the convection velocity of vortex rings increases after they move about one orifice diameter downstream. This is because as the newly formed vortex ring enters the vorticity trail of the former one, the vortex rings will advance at a higher velocity. This feature is seen to be captured well by the simulation.

7.0 CONCLUSIONS

In this study 2D numerical simulations of synthetic jets with a circular orifice were conducted at two diaphragm displacement settings, one representing a typical laminar case and the other a turbulent case. The flow in the cavity was included in the computation in order to provide more accurate predictions. A velocity boundary condition was applied at the neutral position of the diaphragm to account for its temporal deformation. Comparisons were made between the computational results and existing PIV and hot-wire data in terms of the time sequence of the velocity vector field, velocity variations in space and with time.

It is found that computational results for the laminar case agree well with the experimental data. Four turbulent models were tested for the fully turbulent case. It was found that the RNG κ-ε and Standard κ-ω models produced the best match between the computational and experimental results. Finally, the jet peak velocity at the orifice exit at a range of diaphragm oscillation amplitudes and the streamwise trajectory of the cores of vortex rings were also studied and good agreements between the predictions and measurements were found.

This initial study has produced some encouraging evidence for the capacity of FLUENT to simulate the key characteristics of synthetic jets.

ACKNOWLEDGMENTS

The authors would like to thank Dr Zoran Pokusevski for his experimental data. The first author, Hui Tang, would also like to acknowledge the financial support from Manchester University and Universities UK to his PhD studies.

https://doi.org/10.1017/S0001924000000592 Published online by Cambridge University Press

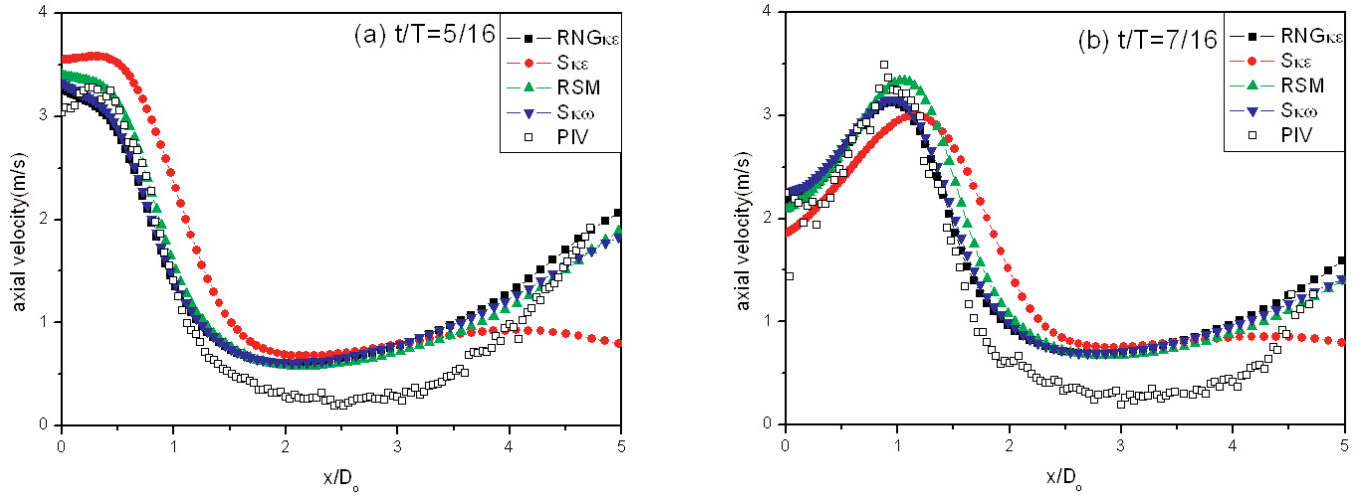


Figure 10. Instantaneous centreline velocity (Case 2).

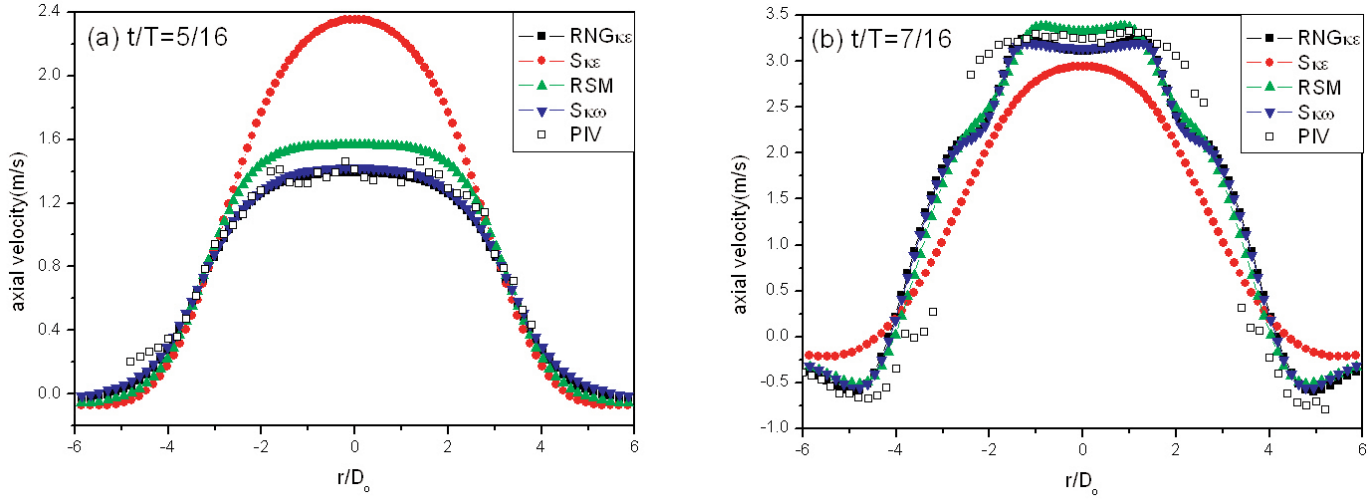


Figure 11. Axial velocity profile at $x = 1D_o$ (Case 2).

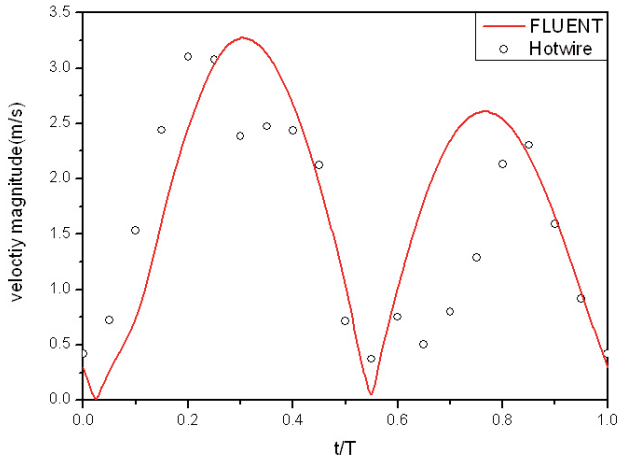


Figure 12. Variation of velocity magnitude at the centre of the orifice exit plane during a cycle (Case 2).

REFERENCES

1. SMITH, B.L. and GLEZER, A. The formation and evolution of synthetic jets, *Physics of Fluids*, 1998, **10**, (9), pp 2281-2297.
2. GLEZER, A. and AMITAY, M. Synthetic jets, *Ann Rev Fluid Mech*, 2002, **34**, pp 503-529.
3. CROOK, A., SADRI, A.M. and WOOD, N.J. The development and implementation of synthetic jets for control of separated flow, 1999, AIAA Paper 99-3176.
4. CROOK, A. and WOOD, N.J. A parametric investigation of a synthetic jet in quiescent conditions, 2000, Ninth International Symposium on Flow Visualization, Edinburgh.
5. ZHONG, S., MULLET, F. and WOOD, N.J. Interaction of synthetic jets with a laminar boundary layer, Seventh Triennial Symposium on Flow Control, Measurement and Visualisation, Italy, August 2003.
6. KRAL, L.D., DONOVAN, J.F., CAIN, A.B. and CARY, A.W. Numerical simulation of synthetic jet actuators, 1997, AIAA Paper 97-1824.
7. RIZZETTA, D.P., VISBAL, M.R., and STANEK, M.J. Numerical investigation of synthetic jet flowfields, *AIAA J*, 1999, **37**, (8), pp 919-927.
8. LEE, C.Y. and GOLDSTEIN, D.B. Two-dimensional synthetic jet simulation, *AIAA J*, 2002, **40**, (3), pp 510-516.

https://doi.org/10.1017/S0001924000000592 Published online by Cambridge University Press

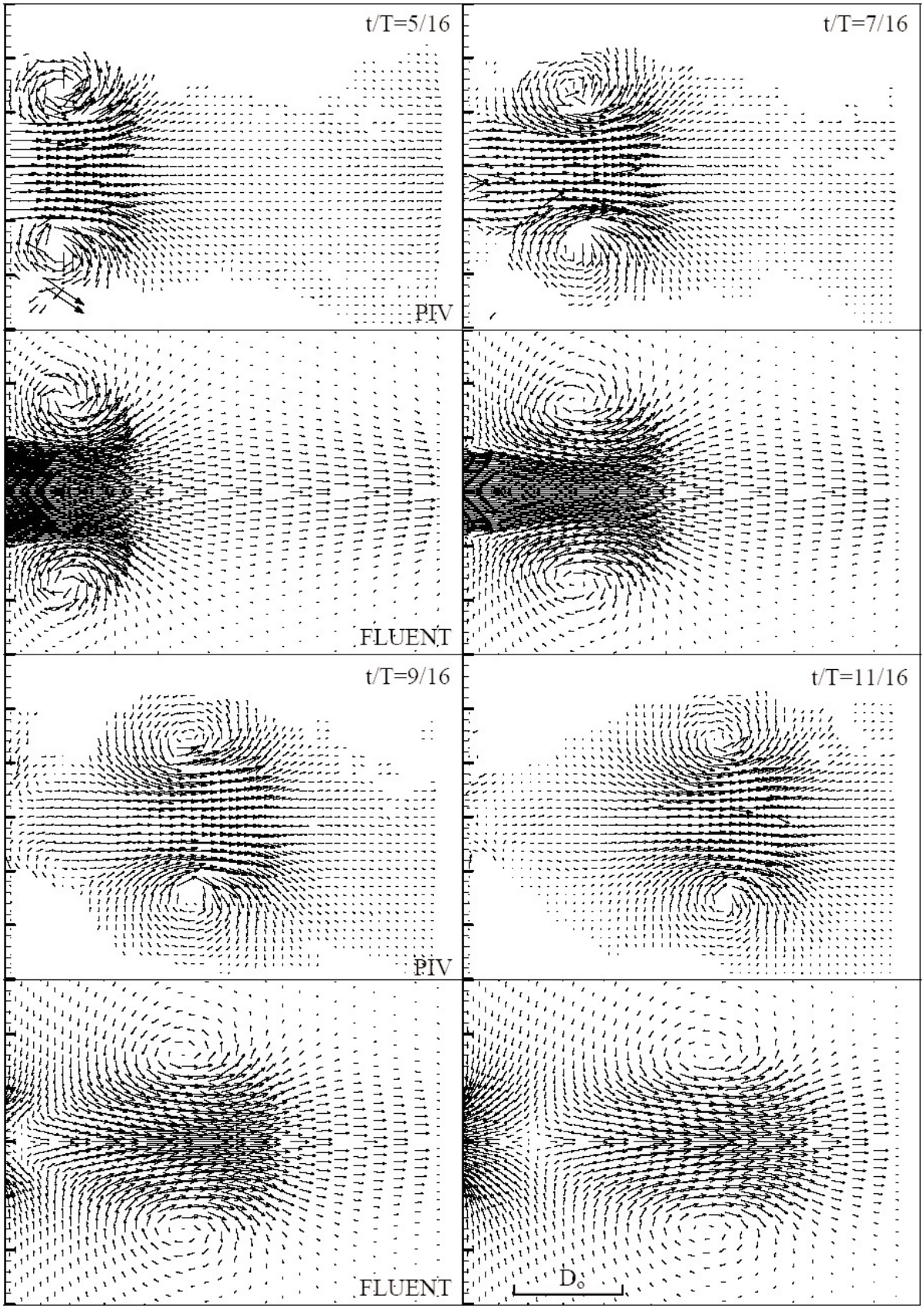


Figure 13. Time sequence of velocity vectors.

https://doi.org/10.1017/S0001924000000592 Published online by Cambridge University Press

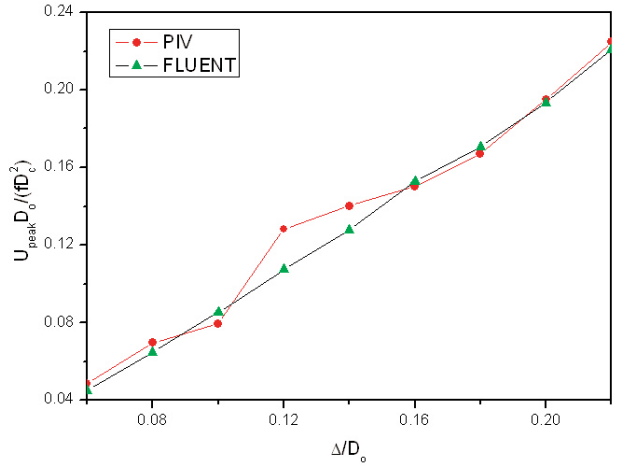


Figure 14. Non-dimensional peak velocities at the orifice exit *versus* diaphragm displacements.

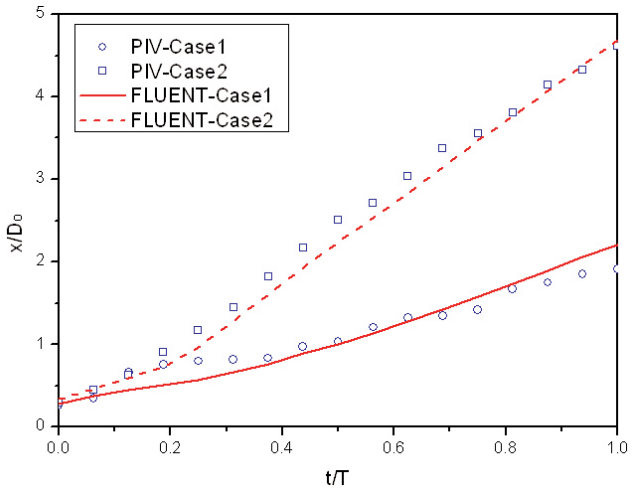


Figure 15. Axial position of vortex rings *versus* time.

9. MALLINSON, S.G., REIZES, J.A., and HONG, G. An experimental and numerical study of synthetic jet flow, *Aeronaut J*, January 2001, **105**, (1043), pp 41-49.
10. MALLINSON, S.G., KWOK, C.Y. and REIZES, J.A. Numerical simulation of micro-fabricated zero mass-flux jet actuators, *Sensor and Actuators A*, 2003, **105**, pp 229-236.
11. TIMOSHENKO and WOINOWSKY-KRIEGER. *Theory of Plates and Shells*, 1959, Second Edition, McGraw-Hill Book Company.

https://doi.org/10.1017/S0001924000000592 Published online by Cambridge University Press